JOURNAL OF APPLIED ELECTROCHEMISTRY 15 (1985) 825–836

Potentiodynamic electrodeposition of paint (EDP)

FRITZ BECK, HARALD GUDER

University-GH-Duisburg, FB6-Elektrochemie, Lotharstr. 65, D-4100 Duisburg 1, West Germany

Received 20 August 1984; revised 3 December 1984

Potentiodynamic electropainting at a rotating iron disc electrode has been investigated with three different EDP resins, two anodic from the acrylate type and one cathodic from the epoxide type, and a wide variation of conditions. Voltage scan rate (v_s = 1 to 200 Vs^{-1}), voltage range (40 to 200 V) and electrode rotation speed (n = 60 and 1000 rpm) were the most important parameters. The (cyclic) voltammetric curves obtained generally exhibit three characteristic features: (1) The current rises steeply at the start of the experiment. Bath resistance transforms the potentiodynamic curve simultaneously into a galvanodynamic curve. After a transition time, τ, a critical pH is attained at the phase boundary and electrocoagulation occurs. This leads to a rapidly decreasing current density. The sharp c.d. maximum thus established has a peak voltage, U_p, which increases with v_s according to the relation $\log U_p \sim 1/3 \log v_s$ in accordance with theory. (2) At high voltages, a limiting current density is observed, increasing with the square root of v_s. This could be quantitatively interpreted in terms of dynamic growth of film thickness governed by Ohmic ion transport in the film. The preceding part of the U/j curve declines with $j \sim t^{-1/2}$, which indicates the prevalence of space charge effects. (3) Ohmic lines are measured in the course of the first reverse scan and in all quasi steady state follow up cycles. They are flatter by a factor of 1000 in regard to the initial Ohmic line and reflect low voltage Ohmic behaviour of the EDP-film. At high voltages positive current deviations occur due to Child's law. The curves can be measured easily and reproducibly. Due to their salient features it is proposed to use them for characterization of EDP-paints.

Nomenclature

a	current density scan rate (mA $cm^{-2} s^{-1}$)
A	electrode area (cm^2)
c^*	critical hydrogen ion- (or hydroxyl ion-) concentration at the electrode for electrocoagulation (mol dm^{-3})
C_A	capacitance of EDP-film per unit area (μF cm^{-2})
E	electric field strength (V cm^{-1})
I	cell current (mA)
j	current density, c.d. (mA cm^{-2})
j_c	capacitance current density (mA cm^{-2})
j_{lim}	limiting current density (mA cm^{-2})
j_p	peak current density (Section 3) (mA cm^{-2})
j_r	residual current density (mA cm^{-2})
j^*	critical current density (for EDP) (mA cm^{-2})
K	constant in Equations 9 and 10 ($V s^{1/2}$)
L_F	thickness of polymer film (cm)
L_{sc}	thickness of space charge layer (cm)
m_e	electrochemical equivalent (g C^{-1})
n_C	exponent in Child's law
n	rotating disc electrode rotation speed (rpm)
N	particle number concentration (cm^{-3})
R_B	bath resistance (Ω)
R_F	film resistance (Ω)
s	density (g cm^{-3})
τ	transition time (s)
U	(cell) voltage (V)
U_{max}	maximum voltage, point of reversion of voltage scan direction (V)
U_p	peak voltage, section 3 (V)
v_s	voltage scan (or sweep) rate ($V s^{-1}$)

0021–891X/85 $03.00 + .12

1. Introduction

Electrodeposition of paint (EDP, 'electrophoretic painting') is an electrochemical process, which has attained great industrial importance in the course of the last twenty years [1]. Today, the first layer (primer) in industrial painting of metal massware is provided by EDP in nearly all cases. Water-born binders, partially neutralized by appropriate solubilizers, constitute the aqueous bath. About six years ago, anodic systems began to be displaced by cathodic ones, offering an improved quality of paint with, for example, improved corrosion protection.

Fundamental electrochemical investigations have often been performed at constant voltage while recording the current–time curve in rough analogy to the industrial process. In some cases, galvanostatic techniques have also been introduced [2–8], sometimes using the rotating disc electrode [2, 3]. However, voltammetric methods, normally applied widely in electrochemistry, have been almost totally neglected up to the present. As the depositing and growing film allows no steady state, (cyclic) potentiodynamic measurements must be used, where the accomplishment of a reproducible quasi steady state seems feasible. The standard theory of voltage sweep methods involves the voltage scan rate v_s

$$v_s = \frac{dU}{dt} \tag{1}$$

as the most prominent parameter [9–13]. The complicated theory is based on a diffusion, and/or reaction controlled Faradayic conversion of the depolarizer. The possibility of application of this theory to the present problem is doubtful.

The only application of this method to EDP has been demonstrated by Bonora *et al.* [14–16]. However, only a narrow variation of parameters was investigated in this work which was limited to aluminium as electrode material, and only a brief attempt at quantitative treatment was offered. Cyclic current voltage techniques have also been used for the investigation of the passivating behaviour of the iron electrode in the EDP process [17], the measurement of current voltage characteristics of the deposited wet film [18–20] and for the examination of the delamination process of organic coatings [21].

It is the objective of this paper to provide for the first time a systematic investigation of the EDP processes by cyclic voltammetry. Voltage range (up to 200 V) and voltage scan rate ($1–200\ V\ s^{-1}$) will be adapted to the problem. Evaluation and quantitative treatment of all parts of the current–voltage curves will be given.

2. Experimental details

We have used two anodic and one cathodic resin in this study. The aqueous solutions contained a concentration of the organic binder in the order of 10 wt %, where bath properties are known to be almost independent of this parameter [3]. The solutions were partially neutralized with an appropriate solubilizer. The bath was used without the addition of pigments. Both anodic polymers were of the acrylate type.

The 'model acrylate', further named MA, was a copolymer of 10% acrylic acid and 90% acrylicacidbutylester. It was neutralized to 81% with dimethylethanolamine to obtain an opaque 7.5 wt % aqueous solution. The same system, but with 10 wt % solutions, was formerly used in most of our fundamental investigations. The other acrylate type resin was Luhydran E 33, abbreviated to E 33, obtained from the BASF company. A 7.3 wt % aqueous dispersion was made according to the data sheet of the manufacturer with the above mentioned solubilizer. The cathodic system was of the epoxide type, neutralized with acetic acid, which we will further call CR.

The degree of neutralization α, and the pH value for the three solutions were

MA: α = 81%, pH = 8.8;
E 33: α = 143%, pH = 9.2;
CR: α = 50%, pH = 6.2.

EDP was performed at a rotating disc electrode, taking into account the great importance of hydrodynamic conditions in the primary electrodeposition process [2, 3]. The electrodes, machined from carbon steel (St 37) with an area, $A = 0.2\ cm^2$, and surrounded by a coaxial polypropylene cylinder, were adapted to the Analytical Rotator ASRP of PINE Instruments

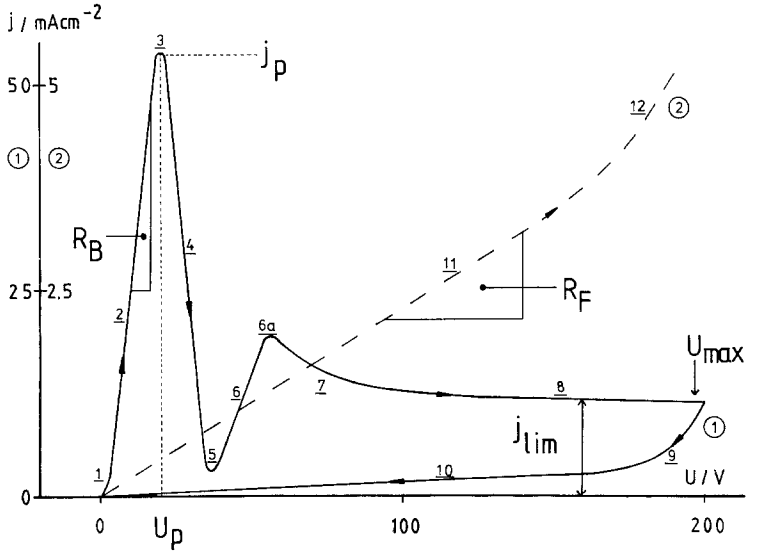

Fig. 1. Schematic representation of cyclic current voltage characteristic for potentiodynamic EDP. Numbered sections 1 through 12 relate to the chronological sequence. ①, ② . . . cycle numbers.

Comp. (Grove City, Pennsylvania, USA). The surface of the disc electrode was polished. Cleaning of the electrode prior to a new experiment was carried out with a tissue paper wetted with acetone as a solvent. The stainless steel counter electrode had an area of 30 cm^2, and was located 2.25 cm below the rotating disc electrode and parallel to it. No reference electrode was used. The electrodes were situated in a 1000 ml cylindrical glass vessel, filled with about 600 ml of EDP bath. All experiments were performed at 20° C. Conversion of bath in the course of the experiments was negligible. Further details concerning the experimental set up are given in [22].

A high voltage scan generator, designed and constructed by the BASF company in Ludwigshafen in 1976, allowed a voltage output between 0 and 200 V at an independent current level up to 0.1 A. The triangular voltage wave function could be run in the range 0.1 to 100 cycles per second. This electronic equipment was modified by adapting an external voltage scan rate control to be operated in a wider range and by introducing the possibility of triggering the voltage sweep. The voltage output was applied directly to the electrochemical cell. Voltage, U, across the cell drove a current $I(t)$ through the cell. Both electrical variables were recorded by means of an xy-recorder ZSK 2 (Rhode and Schwarz).

3. Results

3.1. *Introduction*

The parameters, varied in the work, were

(a) The resin. Three types were used as described above.

(b) The voltage scan rate v_s. This is defined by Equation 1 and was varied over the range of 1 to 200 V s^{-1}.

(c) The voltage range U_{max}. The experiments started at $U = 0$, and voltage scan direction was reversed at a maximum voltage of U_{max}. U_{max} varied from 40 to 200 V.

(d) The rotation speed, n, of the rotation disc electrode. This was not varied systematically (as was done in the course of the previous investigations [2, 3, 23, 24]), but was held constant at two levels: $n = 60$ and 1000 revolutions per min (rpm).

In all cases investigated under the present experimental conditions, a potentiodynamic current voltage curve according to the schematic representation in Fig. 1 was recorded. Initially the current rises roughly linearly with time. Thereafter, it goes through a narrow maximum, which is about one order of magnitude below the current rating of the apparatus. It decreases to a minimum, rises again through a lower and flat maximum and approaches, thereafter, a limiting

current density j_{lim}. On voltage scan reversal, the current collapses rapidly to merge into an Ohmic resistance line at lower voltages. This last part could be reproduced as a steady state in all subsequent cycles, drawn as a dashed curve with a tenfold expanded current scale.

In order to aid the presentation and discussion of the results, numbered sections 1 through 12 have been introduced at salient features of the dynamic current voltage curve, shown in Fig. 1. The first cycle, where the main part of electrodeposition occurs, is drawn with an uninterrupted line; second and subsequent cycles are indicated by dashed lines. Cycle numbers are circled.

3.2. *Variation of voltage scan rate, v_s*

Fig. 2 shows potentiodynamic current–voltage curves for the electrodeposition of model acrylate resin MA at three different voltage scan rates, v_s = 20, 50 and 150 V s^{-1}. For the primary curves the general features already schematically represented in Fig. 1 can clearly be recognized. With increasing v_s, the current peak maximum is shifted to higher current/voltage (j_p/U_p) values. Limiting current densities j_{lim} at

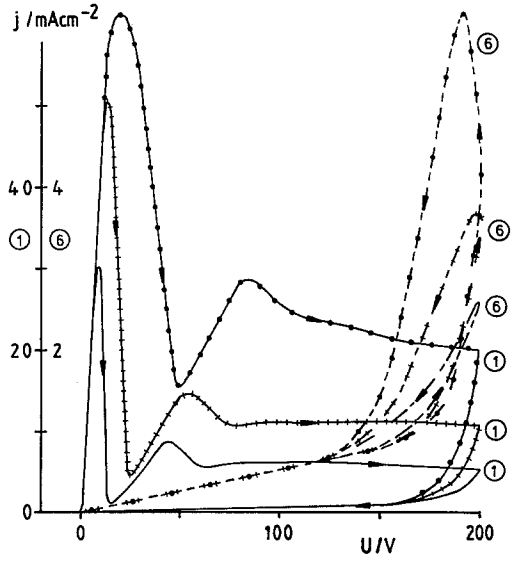

Fig. 2. Cyclic voltammetric curves for potentiodynamic EDP at an iron rotating disc electrode, n = 60 rpm. Bath composition: 7.46 wt % model acrylate MA, neutralized to 81% with dimethylethanoleamine. Variation of voltage scan rate v_s: for cycle ①; v_s, —— 20 V s^{-1}, +++++ 50 V s^{-1}, -·-·- 150 V s^{-1}. For cycle ⑥; v_s, --- 20 V s^{-1}, - - - 50 V s^{-1} and -·-·- 150 V s^{-1}.

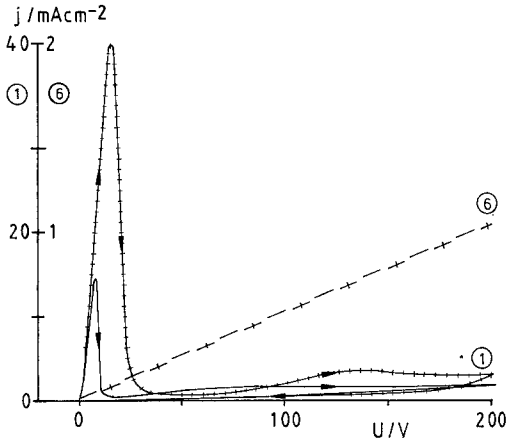

Fig. 3. Cyclic voltammetric curves for potentiodynamic EDP at an iron rotating disc electrode, n = 60 rpm. Bath composition: 15 wt % cathodic resin CR (epoxide type). Variation of voltage scan rate v_s: For cycle ①; v_s, —— 5 V s^{-1} and +++++ 30 V s^{-1}. For cycle ⑥; v_s, --- 5 V s^{-1} and -·-·- 30 V s^{-1}.

higher voltages also increase. The Ohmic regions 10 and 11 (in the second cycle) coincide. However, deviation from Ohm's law in the sixth cycle occurs at a higher voltage level. Hysteresis at that point increases with increasing v_s.

An analogous behaviour was found for the other electropainting systems. Fig. 3 presents the cathodic binder cathodip CR at two different voltage scan rates. Once again, j_p/U_p of the first peak are shifted to higher values with increasing v_s. j_{lim} is lower, and it increases with v_s at a diminished rate.

3.3. *Variation of rotation speed*

An example of the influence of the rotation speed on the voltammetric characteristics is shown in Fig. 4. The industrial acrylate type resin Luhydran E 33 is potentiodynamically deposited at n = 60 rpm and at n = 1000 rpm. Cycles number ①, ② and ⑥ are reproduced. The first cycle is nearly independent of this parameter. The same holds for the sixth cycle, where a quasi steady state has been attained. However, the second cycles deviate very much from each other. The large hysteresis in the case of high rotation speed is indicative of redissolution in the course of the reverse scan.

Similar effects have been found at other voltage scan rates with the same EDP system and with the other acrylate resin MA. The cathodic

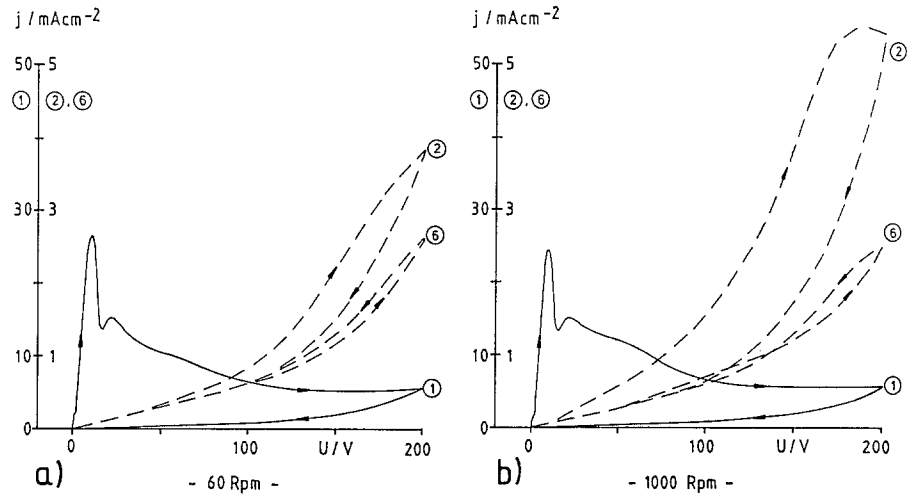

Fig. 4. Cyclic voltammetric curves for potentiodynamic EDP. Bath composition: 7.3 wt % acrylate type resin Luhydran E 33. Voltage scan rate $v_s = 20\,V\,s^{-1}$. The rotating disc electrode (iron) was kept at two different levels of rotation speed n: (a) $n = 60$ rpm and (b) $n = 1000$ rpm. Cycle numbers ①, ② and ⑥ are shown for each of the two measurements.

paint CR proved to be relatively insensitive to rotation speed.

3.4. *Variation of maximum voltage* U_{max}

A sequence of measurements with the model acrylate system MA at a voltage scan rate $v_s = 50\,V\,s^{-1}$ ($n = 60$ rpm) is compiled in Fig. 5. Voltage scan reversal was performed at $U_{max} = 200$, 100, 60 and 40 V, i.e. in the sections 8, 7, 6a and 6. It is a very remarkable feature of these results that the subsequent sections, 9 and 10 do not depend at all on U_{max}. Moreover, the relative length of the Ohmic line 10 in the subsequent cycles is fairly constant. Voltage reversal in the region of low voltages ($U < 50$ V) is under current investigation. These results, deviating distinctly from Fig. 5, will be published elsewhere [22]. At a higher rotation speed, $n = 1000$ rpm, currents in the section 12 of the second cycle are appreciably higher and hysteresis is more pronounced. This is indicative of a higher degree of redissolution [24].

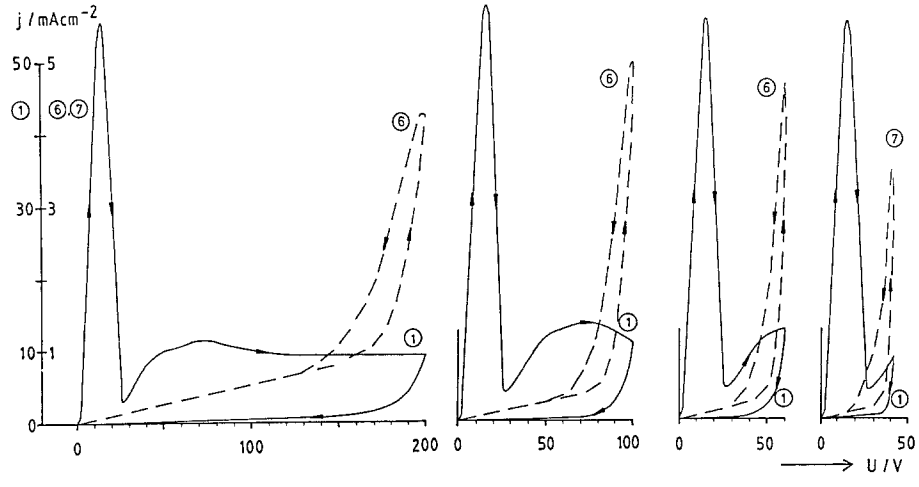

Fig. 5. Cyclic voltammetric curves for potentiodynamic EDP. Bath composition: 7.46% model acrylate MA, voltage scan rate $v_s = 50\,V\,s^{-1}$, $n = 60$ rpm. The maximum voltage, U_{max} was varied from left to right: $U_{max} = 200$, 100, 60 and 40 V. Cycle numbers ① and ⑥ are shown for each set of parameters.

4. Discussion

4.1. *Introduction*

For all voltammetric curves the different features already pointed out in the schematic representation of Fig. 1 have been found. The results are in qualitative agreement with the findings published by Bonora and co-workers [14–16]. In particular, curves for a cathodic paint in a parallel plate Al-electrode configuration, e.g. Fig. 4 in [16], show a very close resemblance to our experimental results.

In the following, the different sections 1 to 12 of our current–voltage curves are discussed, thus following the chronological order of their appearance.

4.2. *Section 1: electrochemical polarization*

We start with an electrochemical couple, blank iron/stainless steel. The voltage is close to zero under the conditions used. Current voltage curves therefore go through the origin. In the early stages of the voltage scan experiment, polarization is negligible due to the similarity of the hydrogen potential at an iron (stainless steel) cathode at medium pH versus iron active dissolution potential. However, if passivation occurs at the anode at higher current densities, the polarization jumps to about 2 V. This effect is responsible for the irregularities in the early stages 1 of the rising current voltage curve, exhibited for all examples reproduced in Figs 2 to 5.

4.3. *Section 2: current limitation by bath resistance R_B*

Bath resistance R_B limits the current in the early stages. The curve degenerates at higher voltages to a resistance line, the slope of which yields R_B:

$$R_B = \left(\frac{\Delta U}{\Delta I}\right)_2 = \frac{1}{A}\left(\frac{\Delta U}{\Delta j}\right)_2 \qquad (2)$$

where A is the area of the rotating disc electrode, to which the measured currents are normalized. In Table 1, these values, varying somewhat unexpectedly with v_s, but not with n, are compared with directly measured R_B values using an alternating current bridge (3 kHz).

4.4. *Section 3: critical $H^+(OH^-)$ concentration*

In section 2, the current density increases linearly with time:

$$j = at \qquad (3)$$

The constant a is the current density scan rate, which can be easily deduced from Equation 1 (in the integrated form) and Equation 2 to be

$$a = \frac{v_s}{AR_B} \qquad (4)$$

Current flow leads to water decomposition as the main electrode process. Thus, at the passive iron anode, protons are injected according to

$$H_2O \longrightarrow 1/2O_2 + 2H^+ + 2e \qquad (5)$$

Oxygen dissolves primarily. Nucleation for the formation of oxygen gas bubbles is greatly retarded in the diffusion layer of extraordinary high viscosity [23, 25].

Protons accumulate in front of the electrode [2, 3]. After a time τ, the critical hydrogen ion concentration c_{H^+}, at the phase boundary is attained and coagulation of the polymer occurs [2, 3, 23, 24, 26].

At constant current density, the time constant, τ, can be calculated using the Sand

Table 1. Determination of bath resistance R_B

Resin	*R_B from Equation 2 (kΩ)*			*R_B (kΩ) directly measured*
	$v_s = 10\,V\,s^{-1}$	$v_s = 30\,V\,s^{-1}$	$v_s = 100\,V\,s^{-1}$	
MA	1.25	1.07	0.94	0.75
E 33	1.4	1.25	1.18	0.99
CR	1.6	1.56	1.35	1.9

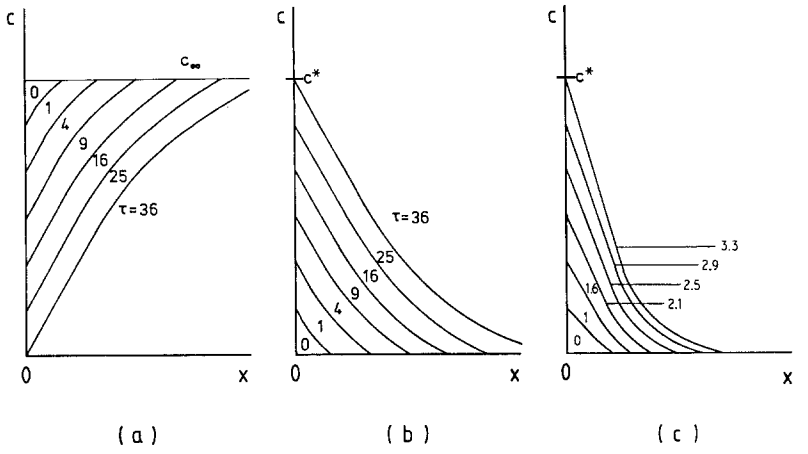

Fig. 6. Schematic representation of concentration profiles in front of an electrode for electroactive species in a nonstirred solution (semi infinite diffusion) (a) being consumed with constant current density (Sand's equation), (b) being generated with constant current density (starting with $c = 0$) and (c) being generated with c.d. increasing linearly with time, j = at. Figures indicate time (in arbitrary units) elapsed since switching on the current. τ = time constant, (a) for attaining $c_0 = 0$, (b, c) for attaining $c_0 = c^*$.

equation,

$$\tau^{1/2} = \tfrac{1}{2}\frac{zFc^*(\pi D)^{1/2}}{j} \qquad (6)$$

This is due to the fact that the time dependent concentration profiles, calculated for consumption of depolarizer at the electrode (for the case of semi-infinite diffusion leading to Equation 6), are exactly symmetrical with the EDP-case of accumulation of depolarizer up to a critical concentration c^*, cf. Fig. 6a and b. This has been experimentally confirmed by the linear increase of $\tau^{-1/2}$ with j [8].

In our case, the galvanostatic experiment is transformed into a galvanodynamic one. The concentration gradient at the surface is no longer constant, but increases linearly with time according to Equation 3. The calculation, presented by several authors for exhaustion of diffusion layer [27–30], once again can be transferred to our problem, cf. Fig. 6c,

$$\tau^{3/2} = \tfrac{3}{4}\frac{zFc^*(\pi D)^{1/2}}{a} \qquad (7)$$

where a is given by Equations 3 and 4.

If we assume that the current maximum 3 corresponds to the transition time τ (establishment of c^* after τ leads to coagulation; the polymer film absorbs the main part of the voltage), then

$$\tau = \frac{U_p}{v_s} \qquad (8)$$

A combination of Equations 4, 7 and 8 leads to ($z = 1$);

$$U_p^{3/2} = [3/4Fc^*(\pi D)^{1/2}R_B A]v_s^{1/2} \qquad (9)$$

Introducing K for the bracketed combination of constants we obtain, after taking logarithms;

$$\log U_p = 2/3 \log K + 1/3 \log v_s \qquad (10)$$

Fig. 7 shows a double logarithmic plot of our experimental results with MA and CR as resins. A straight line with a slope 1/3 can be drawn through the measured points, confirming Equation 10. The experimental points for E 33 are not shown, but they practically coincide with those for MA. From the ordinate section ($\log v_s = 0$), c^* can be derived from K, leading

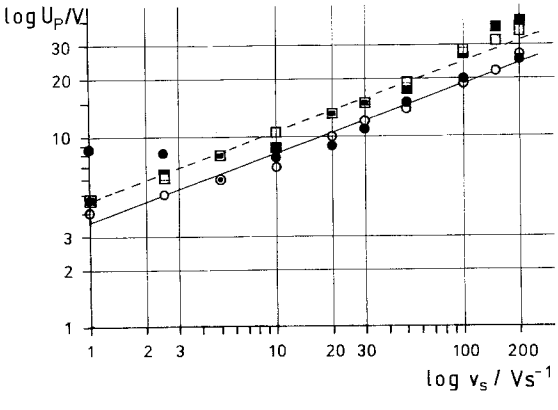

Fig. 7. Increase of first peak voltage U_p with increasing voltage scan rate v_s on a double logarithmic plot for two EDP systems at a rotating iron disc electrode at a rotation speed of n = 60 rpm (empty symbols) and n = 1000 rpm (filled symbols), respectively. ○—● model acrylate MA, □---■ cathodic resin CR.

to pH = 1.6 for MA, which is appreciably lower than the value derived previously [2, 3].

The deviations at low voltage scan rates and high rotation speeds, n, can be rationalized in terms of larger amounts of protons 'escaping' from the diffusion layer prior to reaching c^*. Deviations at high scan rates are due to the competition with time constant of nucleation [2, 26].

4.5. *Sections 4 to 6a: film precipitation and conditioning*

In section 4, the current density decays steeply in spite of further increase of the voltage. A coherent polymer film is precipitated rapidly after the establishment of c^* at point 3. Most of the $H^+(OH^-)$ ions accumulated at that point are consumed by this process.

The current goes through a minimum 5 and rises again 6, going through a second, relatively flat maximum 6a. These sections of the overall current voltage curve cannot be interpreted from the electrical data alone. Additional information must be provided from investigation of film thickness, structure, density and other qualities, but this is outside the scope of the present work. We assume that reorganization and conditioning of the film, freshly precipitated at a very high rate, is responsible for the current/voltage effects in that region. Heating effects are to be excluded: thermal energy is generated in the bath along 1 to 3, where it is easily dissipated. Along 3 to 5, it is generated in the film, but to a decreasing extent. Thus, a new rise of current along 5 to 6a cannot be explained in this manner.

4.6. *Section 7: space charge governed growth of film thickness*

In the section 7 of slowly decreasing current density, a relatively high voltage is applied across a film now compressed due to 'conditioning' and not yet grown to its final thickness. In the high electric field strength established by this way, charge separation in the weakly acid (basic) ion exchange resins must occur [18]. According to Poisson's law, a voltage

$$U = \frac{Ne_0}{2\varepsilon\varepsilon_0} L_{sc}^2 \qquad (11)$$

is absorbed in a space charge layer of thickness L, permittivity $\varepsilon\varepsilon_0$ and space charge density Ne_0 (N = particle concentration of free charge carriers, H^+ or OH^-). From Faraday's law, the rate of growth of the layer thickness is

$$\frac{dL_{sc}}{dt} = \frac{m_e}{s} j \qquad (12)$$

where m_e = electrochemical equivalent and s = density. Integration of Equation 1 leads to

$$U = v_s t \qquad (13)$$

From the last three equations, the following current–time relationship can be derived:

$$j = \frac{s}{m_e}\left(\frac{\varepsilon\varepsilon_0 v_s}{2Ne_0}\right)^{1/2} \frac{1}{(t)^{1/2}} \qquad (14)$$

Actually, a plot of c.d. at 100 V for various resins versus $(v_s)^{1/2}$ shows a proportionality, but with two different slopes, cf. Fig. 8. The slope for the sections at higher voltage scan rates must be now considered further, for only then section 7 is in the region of 100 V, where the necessary high field strength is established.

Calculation of a theoretical slope with the aid of Equation 14 ($m_e = 10^{-2}\,g\,C^{-1}$ [26], $\varepsilon = 10$,

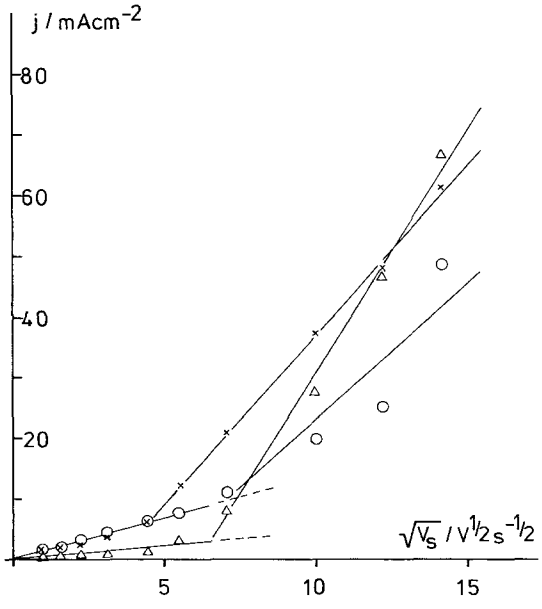

Fig. 8. Linear increase of (limiting) current density (j) with square root of voltage scan rate v_s at U = 100 V. Rotating disc electrode, n = 60 rpm. The EDP-systems used are: o—o MA, x—x E 33, and Δ—Δ CR.

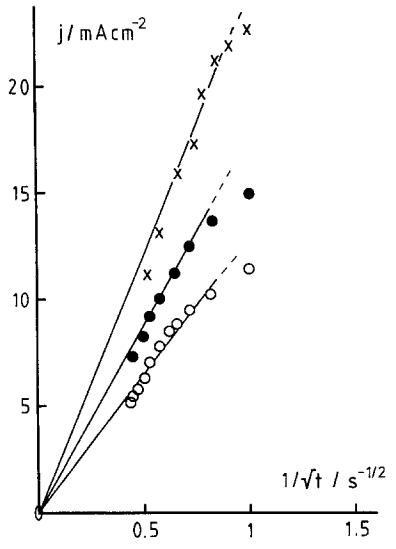

Fig. 9. Evaluation of section 7 (space charge governed growth of film thickness) in a $j/t^{-1/2}$ plot according to Equation 14. Rotating disc electrode, n = 60 rpm, E 33 as EDP system. ○—○ v_s = 20 V s^{-1}, ●—● v_s = 30 V s^{-1} and x—x v_s = 50 V s^{-1}.

t = 10 s (average) and $N = 10^{-9}$ mol cm^{-3} [18]) leads to values in agreement with the experimental slopes of Fig. 8 within one order of magnitude. Thus, the model is satisfactorily confirmed.

In Fig. 9, a plot of the experimental points for E 33 shows a good agreement with the $(t)^{1/2}$-function indicated by Equation 14. The slope (for 20 V s^{-1}) is calculated from Equation 14, to be 3×10^{-2} A s$^{1/2}$ cm^{-2}, taking the same data as above. From Fig. 9, this slope is found to be 1.3×10^{-2} A s$^{1/2}$ cm^{-2} which is in good agreement. Once again the space charge model is confirmed.

4.7. *Section 8: limiting current density* j_{lim}

At even higher voltages, a limiting current density is established. In a simple model, we assume that the film has now grown to a rather extended thickness, and that space charges remain only in a small part of the overall thickness, located at the phase boundary with the bath [18, 26]. Transport in the bulk of the film is governed by Ohm's law:

$$j_{lim} = \kappa E \approx \kappa \frac{U}{L_F} \tag{15}$$

where κ = specific ion conductivity and E = electric field strength. From this equation, an expression for the film thickness growth rate can be derived:

$$\frac{dL_F}{dt} = v_s \frac{\kappa}{j_{lim}} \tag{16}$$

Combination of Equations 12 and 16 leads to

$$j_{lim} = \left(v_s \frac{\kappa s}{m_e}\right)^{1/2} \tag{17}$$

Once again j_{lim} increases with $(v_s)^{1/2}$, as shown by the sections at low voltage scan rate in Fig. 8. Comparison of these experimental values with the theoretical ones obtained from Equation 17 exhibit a surprisingly good agreement, indicating the validity of this simple model, cf. Table 2.

Finally, it must be pointed out, that j_{lim} is about one order of magnitude above the critical current density j^* [3, 23], where electrodeposition starts to be possible. On the other hand, the capacitance current density

$$j_c = C_A v_s \tag{18}$$

calculated with $C_A = 10^{-9}$ F cm^{-2} [18], is lower by six orders of magnitude. Moreover, capacity currents should increase with v_s rather than with $v_s^{1/2}$ as observed experimentally.

The thickness growth of polymer film as an ionic conductor on a metal substrate bears some analogy to the problem of thickness growth of

Table 2. Limiting current density j_{lim} in section 8, at v_s = 10 V s^{-1}

Resin	κ (S cm^{-1})*	j_{lim} (mA cm^{-2}) *calculated from Equation 17*	j_{lim} (mA cm^{-2}) *taken from Fig. 8*
MA	9×10^{-9}	2.9	3.75
E 33	9×10^{-9}	2.9	3.75
CR	10^{-8}	3.2	1.30

* From Table 3, with L_F = 20 μm and A = 0.2 cm^2

oxide films on valve metals [31, 32], as has been pointed out by Pierce *et al.* [33]. Growth of oxide films has been investigated under potentiodynamic conditions too.

4.8. *Section 9: space charge governed decay of current*

On reversal of the voltage sweep direction at U_{max}, the current density decays strongly. This effect is nearly independent of U_{max}, as pointed out in 3.4, cf. Fig. 5. At that point, potentiodynamic growth of the film thickness L_F stops abruptly. However, redissolution does not play any role in this narrow section for several reasons:

(a) There is independence of the effect of resin type, while redissolution is greatly affected by it.
(b) Even under diffusion control [24], the time constant of redissolution (> 10 s) is much larger than time constant of voltage decay (< 1 s).
(c) The flat steady state Ohmic line, traced thereafter, indicates clearly the presence of a coherent film.

The interpretation of the voltage decay must therefore be given in terms of relaxation of the space charge layer in the film. Due to the decreasing medium field strength, charges recombine. Thereafter, normal Ohmic behaviour is exhibited. Similar relaxation effects have been observed with the voltage step method [24, 34].

4.9. *Sections 10 and 11: steady state Ohmic line*

Soon after the relaxation process the curve merges into a normal Ohmic line. Even on the first reverse scan as part of the cyclic curve, a steady state is attained which does not differ practically from the further cycles, cf. Figs 2 to 5.

From the slope of this line, the Ohmic film resistance R_F can be derived:

$$R_F = \left(\frac{\Delta U}{\Delta I}\right)_{10,11} = \frac{1}{A}\left(\frac{\Delta U}{\Delta J}\right)_{10,11} \quad (19)$$

In Table 3, comparable with Table 1, R_F values derived from the slope of potentiodynamic Ohmic lines and those measured directly at the unpolarized film with an alternating current bridge immediately after switching off the voltage, are compiled at three voltage scan rates. Once again, R_F is hardly affected by rotation speed n.

At lower voltages the dynamic current drops well below the critical current density j^*. Nevertheless, redissolution is practically negligible in this region. The situation compares well with the 'residual current' j_r, finally attained in the course of electrodeposition at constant voltage. We interpret this behaviour in terms of neutralization of incoming free base B or acid HA, e.g.

$$B + H^+ \rightleftharpoons BH^+ \quad (20)$$

H^+ originates from the ionic flow through the film at a rate j^*; in the steady state, H^+-ions are injected at the same rate at the phase boundary Fe/film according to Equation 5. In this way, the film is protected from attack by the free solubilizer. We do not believe that at that point, a dynamic equilibrium film redissolution/film deposition is attained [35]. If this were so, the concept of critical H^+–(OH^-–) concentration c^*, proved by several independent methods [24, 26], would loose its physical significance.

4.10. *Section 12: Child's law*

Returning to high voltages at 12 in the course of

Table 3. Determination of film resistance R_F, cycle ⑤

Resin	*R_F from Equation 19 ($M\Omega$)*			*R_F ($M\Omega$) directly measured*
	$v_s = 10\,V\,s^{-1}$	$v_s = 30\,V\,s^{-1}$	$v_s = 100\,V\,s^{-1}$	
MA	0.95	0.93	0.88	1
E 33	0.90	0.91	0.93	1
CR	0.98	0.99	0.85	0.9

cycles ②, ③ . . . , appreciable positive deviations from Ohm's law have been observed. The current rise is more than proportional to the voltage. Our former evaluation of MA behaviour [18] led to a current–voltage relationship (at a constant L)

$$j = BU^{n_C} \tag{21}$$

where B was a consant and n_C was found to be between 5 and 7. This corresponds to Child's law, valid for charge transport in a space charge layer with traps cf. [36]. n_C will be two for normal charge injection into a space charge layer of constant space charge density. An *ab initio* model was presented in [18].

In addition to this effect, the current rises due to some redissolution of the film at very small voltages. This view agrees well with our model presented in Section 4.9, for the 'protection mechanism' of neutralizing incoming solubilizer looses its validity with decreasing c.d. ($j \to 0$, $j \ll j^*$). Under these conditions, the current density will rise to j_{lim}, especially at high n_C and at low v_s. This is clearly indicated by the exemplary curves reproduced in Figs 2 to 5. Large hystersis effects are observed under superposition of both effects.

5. Conclusions

Our systematic investigation of potentiodynamic EDP leads us to well differentiated and structured voltammetric curves. They are characterized by a primary steep current peak (at low voltages) and a limiting current density at high voltages. Starting with the second cycle, quasi steady state Ohmic lines are established in almost the whole range of voltages.

The measuring technique is very common in electrochemistry. If a high voltage triangular voltage generator is available, measurements can be performed easily and rapidly. A two-electrode arrangement is feasible, for polarization is small compared with cell voltage. This should facilitate introduction of such an experimental technique in paint laboratories. Moreover, simple stationary electrodes seem also to be feasible, since our experiments at the rotating disc electrode demonstrated virtually no influence of rotation speed under most experimental conditions.

The method seems to be well suited to characterization of EDP-resins. (Correspondence to parameters of technical significance has been pointed out in the Discussion.) The curves have more pronounced features than curves derived from the usual chronoamperometry or chronopotentiometry. Reproducibility of the curves is quite satisfactory. Finally, correspondence with the industrial process, where voltage is often stepped rather than constant, is remarkably close.

Acknowledgements

A financial grant to one of us (HG) and material assistance by BASF Farben und Fasern AG, Hiltrup, is gratefully acknowledged. We wish to thank Drs Batzill, Heilmann and Streitberger, Hiltrup, as well as Sabelus and Spoor, Ludwigshafen, for practical support, predominantly in regard to provision of EDP resins. Dr G. Jansen, BASF Ludwigshafen and Dr Krohn from this laboratory helped us greatly in design, construction and further development of the electronic high voltage triangle wave generator.

References

[1] G. E. F. Brewer, *J. Appl. Electrochem.* **13** (1983) 269.
[2] F. Beck, *Farbe und Lack* **72** (1966) 218.
[3] F. Beck, *Chem.-Ing.-Techn.* **40** (1968) 575.
[4] D. Saatweber and B. Vollmert, *Angew. Makromol. Chem.* **8** (1969) 1.
[5] Y. Nakamura, S. Ando and H. Nozaki, *J. Electrochem. Soc. Jpn.* **37** (1969) 13.
[6] J. P. Giboz and J. Lahaye, *J. Paint Technol.* **43** (1971) 79.
[7] Z. Kovač-Kalko in 'Electrodeposition of Coatings', edited by G. E. F. Brewer (American Chemical Society, Washington, 1973) p. 149.
[8] C. Catonne and J. Royon, Proc. Interfinish Basel 1972, Forster Verlag, Zürich, p. 258, 1973.
[9] R. S. Nicholson and I. Shain, *Anal. Chem.* **36** (1964) 706.
[10] *Idem, ibid.* **37** (1965) 178.
[11] *Idem, ibid.* **37** (1965) 190.
[12] E. R. Brown and R. F. Large, in 'Physical Methods of Chemistry', Part II A, Chapter 6, edited by A. Weissberger and B. W. Rossiter, (Wiley Interscience, New York, 1971).
[13] A. J. Bard and L. R. Faulkner, 'Electrochemical Methods', Chapter 6, (J. Wiley, New York, 1980).
[14] P. L. Bonora and R. Calvillo, *Proceed. Interfinish*, 1976.
[15] G. Trombetti, G. Bianchini and P. L. Bonora, *Pitture e Vernici* **2** (1977) 3.
[16] P. L. Bonora, R. Calvillo, G. Trombetti and G. Bianchini, Proceed. Fatipec Congress (1978) 171.

[17] C. A. May and G. Smith, *J. Paint Techn.* **40** (1968) 494.
[18] F. Beck, *Ber. Bunsenges. Phys. Chem.* **72** (1968) 445.
[19] B. A. Cooke and T. A. Strivens, *J. Oil Colour Chem. Assoc.* **51** (1968) 344.
[20] B. A. Cooke, *Paint Technol.* **34** (1970) 12.
[21] H. Leidheiser Jr and M. W. Kendig, *Ing. Eng. Chem. Prod. Res. Dev.* **17** (1978) 54.
[22] H. Guder and F. Beck, *Farbe und Lack* **91** (1985) 388.
[23] F. Beck, *Oberfläche Surface* **14** (1973) 73.
[24] *Idem, Pitture e Vernici* October (1983) 15.
[25] F. Beck and H. Guthke, *Farbe und Lack* **77** (1971) 299.
[26] F. Beck, *Progr. in Org. Coatings* **4** (1976) 1.
[27] T. Kambara and I. Tachi, *J. Phys. Chem.* **61** (1957) 1405.
[28] W. H. Reinmuth, *Anal. Chem.* **32** (1960) 1509.
[29] R. C. Bowers, G. Ward, C. M. Wilson and D. D. DeFord, *J. Phys. Chem.* **65** (1961) 672.
[30] R. W. Murray and Ch. N. Reilley, *J. Electroanal. Chem.* **3** (1962) 64.
[31] L. Young, 'Anodic Oxide Films' (Academic Press, New York, 1961).
[32] M. J. Dignam in 'Comprehensive Treatise of Electrochemistry', Vol. 4, edited by J. O'M. Bockris *et al.*, (Plenum Press, New York, 1981) p. 247 ff.
[33] P. E. Pierce, Z. Kovač, and C. Higginbotham, Proceed. Fatipec Congress XIV, 119 (1978).
[34] B. A. Cooke, N. M. Ness and A. L. L. Palluel, in A. T. Kuhn, 'Industrial Electrochemical Processes' (Elsevier, Amsterdam, 1971) p. 417.
[35] P. E. Pierce, *J. Coat. Techn.* **53** (1981) 52.
[36] H. Gerischer, in 'Physical Chemistry, An Advanced Treatise', Vol. IX A, edited by H. Eyring, (Academic Press, New York, 1970) pp. 507–509.